Journal of Geodesy (1998) 72: 578–585

Journal of Geodesy
© Springer-Verlag 1998

Fast integration of low orbiter's trajectory perturbed by the earth's non-sphericity

C. Hwang, M.-J. Lin

Department of Civil Engineering, National Chiao Tung University, 1001 Ta Hsueh Road, Hsinchu 30050, Taiwan, ROC
Fax: +886 3 5716257; e-mail:hwang@geodesy.cv.nctu.edu.tw

Received: 28 July 1997 / Accepted: 1 April 1998

Abstract. A fast algorithm is proposed to integrate the trajectory of a low obiter perturbed by the earth's non-sphericity. The algorithm uses a separation degree to define the low-degree and the high-degree acceleration components, the former computed rigorously, and the latter interpolated from gridded accelerations. An FFT method is used to grid the accelerations. An optimal grid type for the algorithm depends on the trajectory's permissible error, speed, and memory capacity. Using the non-spherical accelerations computed from EGM96 to harmonic degree 360, orbit integrations were performed for a low orbiter at an altitude of 170 km. For a separation degree of 50, the new algorithm, together with the predict-pseudo correct method, speeds up the integration by 145 times compared to the conventional algorithm while keeping the errors in position and velocity below 10^{-4} m and 10^{-7} m/s for a 3-day arc.

Key words. Orbit integration · FFT · Perturbation · Spherical harmonics

1 Introduction

There are many satellite missions that require the use of low orbiters. For example, the high-low scenario of a satellite-to-satellite tracking mission, a satellite gradiometry mission, and the recently approved GRACE mission (CSR 1997; see also the review in Seeber 1993). In the trajectory prediction of a low orbiter, the biggest challenge comes from the highly time-consuming computation of the accelerations due to the earth's nonspherical perturbation. In the past this problem has been noticed and some useful techniques such as those described in Balmino et al. (1990) and Balmino and Barriot (1990) have been proposed. This paper pursues the subject further and proposes a fast algorithm based on the facts (1) that the trajectories of most geodetic satellites are near circular and hence their ranges of motion in the radial direction (called radial range for short) are small, and (2) that a predicted trajectory allows some degree of error. For example, based on real data, it is found that the radial ranges of TOPEX/POSEIDON and Geosat are about 40 km (between 7695 and 7735 km) and about 50 km (between 7140 and 7190 km), respectively. For a near-circular low orbiter, the radial range is even smaller. In the following development, the basis of the proposed algorithm and formulae for relevant computations will be presented. The algorithm is then applied to a satellite orbiting at an altitude of 170 km to study the efficiency of the algorithm. In all the following computations/experiments we use the IEEE double-precision arithmetic and scalar machines without parallel computing facility.

2 Accelerations due to earth's nonspherical perturbation

There are numerous forces acting on a low earth orbiter, see, e.g., Seeber (1993) and Tapley (1989). In this paper, the only force considered is that due to the earth's nonspherical perturbation. Also, only basic formulae needed in developing the proposed algorithm will be mentioned. The potential of the earth's nonspherical perturbation can be expanded into a series of spherical harmonics as (Heiskanen and Moritz, 1967)

$$V_{NS}(r,\phi,\lambda) = \frac{\mu}{r}\sum_{n=2}^{\infty}\left(\frac{a_e}{r}\right)^n \sum_{m=0}^{n}(\bar{C}_{nm}\cos m\lambda + \bar{S}_{nm}\sin m\lambda) \times \bar{P}_{nm}(\sin\phi) \quad (1)$$

where $\mu = GM$ is the product of the gravitational constant and the earth's mass, r, ϕ, λ are the spherical

Correspondence to: Chenway Hwang

coordinates (geocentric distance, geocentric latitude, and longitude), a_e is a scaling factor approximately equal to the semi-major axis of a reference ellipsoid, $\bar{C}_{nm}$ and $\bar{S}_{nm}$ are the spherical harmonic coefficients, and $\bar{P}_{nm}(\sin\,\phi)$ is the fully normalized associated Legendre function of degree n and order m. The acceleration vector expressed in the earth-fixed coordinate system is

$$\bar{a}^b = \begin{bmatrix} \frac{\partial V_{NS}}{\partial x_b} \\ \frac{\partial V_{NS}}{\partial y_b} \\ \frac{\partial V_{NS}}{\partial z_b} \end{bmatrix} = \begin{bmatrix} \frac{\partial r}{\partial x_b} & \frac{\partial \phi}{\partial x_b} & \frac{\partial \lambda}{\partial x_b} \\ \frac{\partial r}{\partial y_b} & \frac{\partial \phi}{\partial y_b} & \frac{\partial \lambda}{\partial y_b} \\ \frac{\partial r}{\partial z_b} & \frac{\partial \phi}{\partial z_b} & \frac{\partial \lambda}{\partial z_b} \end{bmatrix} \begin{bmatrix} \frac{\partial V_{NS}}{\partial r} \\ \frac{\partial V_{NS}}{\partial \phi} \\ \frac{\partial V_{NS}}{\partial \lambda} \end{bmatrix} \tag{2}$$

where x_b, y_b, and z_b are the earth-fixed coordinates, and

$$\frac{\partial V_{NS}}{\partial r} = -\frac{\mu}{r^2}\sum_{n=2}^{\infty}\left(\frac{a_e}{r}\right)^n (n+1) \sum_{m=0}^{n}(\bar{C}_{nm}\cos\,m\lambda + \bar{S}_{nm}\sin\,m\lambda)\bar{P}_{nm}(\sin\,\phi) \tag{3}$$

$$\frac{\partial V_{NS}}{\partial \phi} = \frac{\mu}{r}\sum_{n=2}^{\infty}\left(\frac{a_e}{r}\right)^n \sum_{m=0}^{n}(\bar{C}_{nm}\cos\,m\lambda + \bar{S}_{nm}\sin\,m\lambda)\cdot \left[\sqrt{(n-m)(n+m+1)(1+\delta(m))}\,\bar{P}_{n,m+1}(\sin\,\phi) - m\tan\,\phi\bar{P}_{nm}(\sin\,\phi)\right] \tag{4}$$

$$\frac{\partial V_{NS}}{\partial \lambda} = \frac{\mu}{r}\sum_{n=2}^{\infty}\left(\frac{a_e}{r}\right)^n \sum_{m=0}^{n} m(\bar{S}_{nm}\cos\,m\lambda - \bar{C}_{nm}\sin m\lambda) \times \bar{P}_{nm}(\sin\,\phi) \tag{5}$$

with $\delta(m) = 1$ for $m = 0$, and $\delta(m) = 0$ for $m \neq 0$. Since orbit integration must be performed in the inertial coordinate system, it is necessary to transform $\bar{a}^b$ to a vector expressed in the inertial coordinate system. In this paper, we simplify the transformation by neglecting precession, nutation, and polar motion and obtain the acceleration vector expressed in the inertial coordinate system:

$$\bar{a}^I = \begin{bmatrix} \frac{x}{r} & \frac{-xz}{r\sqrt{x^2+y^2}} & \frac{-y}{\sqrt{x^2+y^2}} \\ \frac{y}{r} & \frac{-yz}{r\sqrt{x^2+y^2}} & \frac{x}{\sqrt{x^2+y^2}} \\ \frac{z}{r} & \frac{\sqrt{x^2+y^2}}{r} & 0 \end{bmatrix} \begin{bmatrix} \frac{\partial V_{NS}}{\partial r} \\ \frac{\partial V_{NS}}{r\,\partial \phi} \\ \frac{\partial V_{NS}}{r\,\cos\,\phi\partial \lambda} \end{bmatrix} = M\bar{a} \tag{6}$$

where $\overline{x, y, z}$ are the inertial coordinates, $r = \sqrt{x^2 + y^2 + z^2}, M$ is an orthogonal matrix and $\bar{a}$ is the acceleration vector expressed in a local rotating frame. The geocentric latitude and longitude can be computed from

$$\phi = \sin^{-1}\frac{z}{r}, \lambda = \tan^{-1}\frac{y}{x} - \text{GAST} \tag{7}$$

where GAST is the Greenwich apparent sidereal time.

3 Satellite altitude and average power of acceleration

Depending on the satellite altitude, the upper bound of the degree, which is theoretically ∞, in the spherical harmonic expansion given by Eq. (1), can be replaced by a cutoff degree. This is due to the factor $(\frac{a_e}{r})^n$ in Eq. (1) that attenuates the magnitude of satellite acceleration and due to the asymptotic decrease in the $\bar{C}_{nm}$ and $\bar{S}_{nm}$ coefficients. The cutoff degree can be obtained by investigating the average power of satellite acceleration over a sphere at the satellite's altitude according to the theory adopted below. From Eq. (6) we have

$$\bar{a} = \begin{bmatrix} \frac{\partial V_{NS}}{\partial r} \\ \frac{\partial V_{NS}}{\partial \phi} \\ \frac{\partial V_{NS}}{r\,\cos\,\phi\partial \lambda} \end{bmatrix} = \begin{bmatrix} A_r \\ A_\phi \\ A_\lambda \end{bmatrix} \tag{8}$$

where A_r, A_ϕ, and A_λ are the radial, latitudinal, and longitudinal accelerations, respectively. Since A_ϕ and A_λ lie on a plane perpendicular to the radial direction, the two form the horizontal acceleration. Assuming the expansion in Eq. (1) is up to degree K, the average power of $\bar{a}$ over a sphere of radius R (R is approximately equal to the earth's mean radius plus the satellite mean altitude) is

$$P_K = \frac{1}{4\pi}\int_\sigma |\bar{a}|^2\,\mathrm{d}\sigma = \frac{1}{4\pi}\int_\sigma A_r^2\,\mathrm{d}\sigma + \frac{1}{4\pi}\int_\sigma (A_\phi^2 + A_\lambda^2)\,\mathrm{d}\sigma \tag{9}$$

where σ is the sphere of radius R, and $\mathrm{d}\sigma = \cos\,\phi\,\mathrm{d}\phi\,\mathrm{d}\lambda$. With the orthogonality relationship of spherical harmonics (Heiskanen and Moritz 1967) the average power of the radial acceleration is

$$\frac{1}{4\pi}\int_\sigma A_r^2\,\mathrm{d}\sigma = \left(\frac{\mu}{R^2}\right)^2 \sum_{n=2}^{K}\left(\frac{a_e}{R}\right)^{2n}(n+1)^2\sum_{m=0}^{n}(\bar{C}_{nm}^2 + \bar{S}_{nm}^2) \tag{10}$$

Using the following property of spherical harmonics (Hwang 1998)

$$\frac{1}{4\pi}\int_\sigma \nabla Y_{nm}^\alpha \cdot \nabla Y_{sr}^\beta\,\mathrm{d}\sigma = \begin{cases} n(n+1), & \text{if } \alpha = \beta \text{ and } n = s \text{ and } m = r \\ 0, & \text{otherwise} \end{cases} \tag{11}$$

where

$$\nabla = \left(\frac{\partial}{\partial\phi}\frac{\partial}{\cos\,\phi\,\partial\lambda}\right) \tag{12}$$

and

$$Y_{nm}^\alpha(\phi,\lambda) = \begin{bmatrix} \bar{P}_{nm}(\sin\,\phi)\cos\,m\lambda, \alpha = 0 \\ \bar{P}_{nm}(\sin\,\phi)\sin\,m\lambda, \alpha = 1 \end{bmatrix} \tag{13}$$

we get the average power of the horizontal acceleration:

$$\frac{1}{4\pi}\int_{\sigma}(A_{\phi}^{2}+A_{\lambda}^{2})\,\mathrm{d}\sigma=\frac{1}{4\pi R^{2}}\int_{\sigma}(\nabla V_{NS}\cdot\nabla V_{NS})\,\mathrm{d}\sigma$$
$$=\left(\frac{\mu}{R^{2}}\right)^{2}\sum_{n=2}^{K}\left(\frac{a_e}{R}\right)^{2n}n(n+1)$$
$$\sum_{m=0}^{n}(\bar{C}_{nm}^{2}+\bar{S}_{nm}^{2}) \tag{14}$$

Thus,

$$P_K=\left(\frac{\mu}{R^{2}}\right)^{2}\sum_{n=2}^{k}\left(\frac{a_e}{R}\right)^{2n}(n+1)(2n+1)\sum_{m=0}^{n}(\bar{C}_{nm}^{2}+\bar{S}_{nm}^{2}) \tag{15}$$

From Eqs. (10) and (14), the average power of the radial acceleration is larger than that of the horizontal acceleration.

With a specified error tolerance the cutoff degree can be determined by comparing the power of acceleration up to the cutoff degree and the "total" power of acceleration. We assume that the total power of acceleration can be obtained by an expansion to a very high degree $N_{\max}$. Currently, $N_{\max}=360$ is the highest possible degree, and is used in, e.g., the OSU91A model (Rapp et al. 1991) and the EGM96 model (Lemoine et al. 1997). To this end, one may compute the relative power up to degree K:

$$\rho_K=\frac{P_K}{P_{N_{\max}}} \tag{16}$$

We should have $\rho_K\approx 1$ for K to be the cutoff degree. Figure 1 shows the values $\log_{10}(1-\rho_K)$ at different altitudes with $N_{\max}=360$ and the geopotential coefficients from the EGM96 model. From Fig. 1, we find that the K values for a low orbiter at altitude = 170 km, TOPEX/POSEIDON and GPS satellites to reach the condition $(1-\rho_K)\approx 10^{-14}$ are 354, 54, and 8, respectively, which can be used as the cutoff degrees for the corresponding satellites in the IEEE double-precision environment.

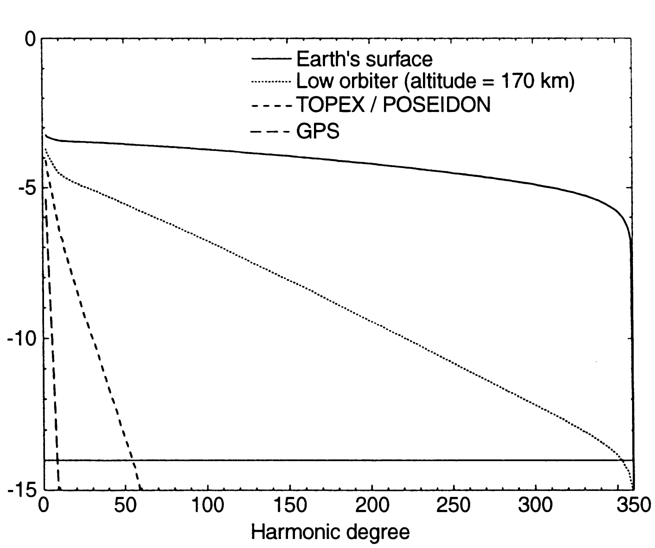

Fig. 1. The values $\log_{10}(1-\rho_K)$ vs. spherical harmonic degree, ρ_K is the relative power up to degree K

4 Computing accelerations by parts

4.1 The separation degree

The key to the proposed algorithm is that, with the spherical harmonic expansions, the three accelerations, A_r, A_ϕ, and A_λ, can be decomposed into a low-degree and a high-degree components which have different magnitudes and can be computed with different methods. To see this, we define the relative partial power from degrees $K1$ to $K2$ as

$$\rho_{K1-K2}=\frac{P_{K2}-P_{K1-1}}{P_{N_{\max}}},K1<K2 \tag{17}$$

Again, using $N_{\max}=360$ and the geopotential coefficients from the EGM96 model, we computed the relative partial powers over different ranges of harmonic degrees at an altitude of 170 km, as shown in Table 1. Table 1 suggests that, compared to the low-degree component, the high-degree component contributes very little to the total acceleration. For example, the acceleration due to the components from degrees 51 to 360 is only about 3×10^{-6} of the total acceleration.

Let A_i be any of the three accelerations $A_r, A\phi$, and A_λ. At an appropriate harmonic degree S, the total acceleration can be decomposed into the low-degree component, A_i^L, and the high-degree component, A_i^H as

$$A_i=\sum_{n=2}^{S}\sigma_n^i+\sum_{n=S+1}^{N_{\max}}\sigma_n^i=A_i^L+A_i^H,\ i=1,2,3 \tag{18}$$

where σ_n^i is the degree-n component of the acceleration. In Eq. (18) S is the *separation degree*. Given a permissible error of A_i, we can compute A_i^L rigorously while computing A_i^H by an approximate and fast method. Let e and e^H be the relative errors of A_i and A_i^H, respectively. The absolute error of A_i will come entirely from A_i^H, namely,

$$eA_i=e^H A_i^H \tag{19}$$

Table 1. Relative partial powers from harmonic degrees $K1$ to $K2$ at an altitude of 170 km

$K1$	$K2$	ρ_{K1-K2}
2	50	$0.9997997402e+0$
2	70	$0.9999970705e+0$
2	180	$0.9999999987e+0$
51	70	$0.1992062613e-5$
51	180	$0.2928163588e-5$
51	360	$0.2929420279e-5$
71	180	$0.9361009758e-6$
71	360	$0.9373576658e-6$
181	360	$0.1256689991e-8$

Let $A_i = \alpha A_i^H \approx A_i^L$, where α is a large number. From Eq. (19), we have

$$\alpha = \frac{e^H}{e} \tag{20}$$

which gives the criterion for selecting S. For example, given $e = 10^{-12}$ and $e^H = 10^{-6}$, we should choose an S so that the low-degree acceleration component is 10^6 of the high-degree acceleration component. In this example, the smallest possible S for an altitude of 170 km will be 50, see also Table 1.

4.2 Computing gridded high-degree accelerations

A procedure to compute A_i^H with some degree of error is: (1) compute A_i^H at regular grids over all possible ranges of satellite motion in the r, ϕ, and λ directions, then (2) interpolate the needed A_i^H values at the required locations. For the first step, the radial range can be determined by integrating the orbit with the low-degree acceleration component A_i^L. This only needs to be done once for the entire phase of a satellite mission, and the computational time is negligible. The range of λ is from 0° to 360° and the range of ϕ is from $-I_{\max}$ to $I_{\max}$, where $I_{\max}$ is the maximum value of the satellite inclination. The gridded A_i^H values can be computed by Fast Fourier transform (FFT). The general expression for computing A_i^H on a sphere of radius R by FFT is:

$$\begin{aligned} A_i^H(R,\phi,\lambda) &= \sum_{m=0}^{N_{\max}} \left\{ \left[\sum_{n=L}^{N_{\max}} \beta_{nm}^i(R,\phi)\bar{C}_{nm} \right] \cos m\lambda \right. \\ &\quad \left. + \left[\sum_{n=L}^{N_{\max}} \beta_{nm}^i(R,\phi)\bar{S}_{nm} \right] \sin m\lambda \right\} \\ &= \sum_{m=0}^{N_{\max}} (C_m \cos m\lambda + S_m \sin m\lambda) \end{aligned} \tag{21}$$

where

$$L = \begin{cases} S, & \text{if } m \le S \\ m, & \text{if } m > S \end{cases} \tag{22}$$

and the explicit expression for $\beta_{nm}^i(R,\phi)$ can be found by comparing Eq. (21) with Eqs. (3), (4), and (5). If we wish to compute A_i^H along a parallel with a step of $\Delta\lambda$, the number of data grids is $N = 2\pi/\Delta\lambda$. Setting $C_m = S_m = 0$ for $m = N_{\max}+1,\ldots,N-1$, the formula equivalent to Eq. (21) suitable for FFT is

$$A_i^H(R,\phi,k\Delta\lambda) = \sum_{m=0}^{N-1} (C_m \cos\frac{2\pi mk}{N} + S_m \sin\frac{2\pi mk}{N}), \quad k = 0,\ldots,N-1 \tag{23}$$

If we set

$$B_0 = C_0, B_m = \frac{C_m - iS_m}{2}, B_{-m} = \frac{C_m + iS_m}{2}, \quad i = \sqrt{-1}, m = 1,\ldots,N-1 \tag{24}$$

Eq. (23) becomes

$$\begin{aligned} A_i^H(R,\phi,k\Delta\lambda) &= \sum_{m=0}^{N-1} B_m e^{i2\pi mk/N} \\ &\quad + \sum_{m=-(N-1)}^{0} B_m e^{i2\pi mk/N} - B_0 \\ &= P + P^* - B_0 = 2\mathrm{Re}(P) - B_0 \end{aligned} \tag{25}$$

where $P = \sum_{m=0}^{N-1} B_m e^{i2\pi mk/N}$ can be computed by FFT (see, e.g., Press et al. 1989). A fixed R in Eq. (25) corresponds to a layer of gridded A_i^H values. The speed-up comes from the fact that all gridded values along the same parallel can be computed simultaneously by FFT. Furthermore, by the property of the associated Legendre function

$$\bar{P}_{nm}(-\sin\phi) = (-1)^{n+m}\bar{P}_{nm}(\sin\phi) \tag{26}$$

it is advantageous to choose a grid interval along meridian, $\Delta\phi$, so that 90° is an integer multiplier of $\Delta\phi$. That is, the parallels where gridded A_i^H values are wanted are symmetric with respect to the equator, so that by Eq. (26) the associated Legendre functions need only be computed once for the two symmetric parallels situated at the northern and the southern hemispheres, see also Colombo (1981). For the case $N_{\max} = 360$ and $S = 50$, the speed-up factors achieved by the FFT method as compared to the termwise evaluation of the harmonic series are given in Table 2. Clearly, the efficiency of the FFT method increases as the grid interval $\Delta\phi \times \Delta\lambda$ decreases.

Grid intervals in the radial, latitudinal, and longitudinal directions, $\Delta r, \Delta\phi, \Delta\lambda$, and the method of interpolation will determine the accuracy of the interpolated A_i^H values at the required locations. Based on Fig. 1, for an altitude lower than 200 km we need to compute accelerations almost up to $N_{\max}$. If $N_{\max}$ is used, then the maximum allowable grid intervals in ϕ and λ for "reproducing" the acceleration at any point from the gridded accelerations are $\pi/N_{\max}$. Thus, for a low orbiter $\Delta\phi$ and $\Delta\lambda$ should fulfill the condition

$$\Delta\phi \le \frac{\pi}{N_{\max}} \text{ and } \Delta\lambda \le \frac{\pi}{N_{\max}} \tag{27}$$

Since the average power of the radial acceleration is greater than that of the horizontal acceleration [compare Eqs. (10) and (14)], the radial grid interval should be less than the horizontal grid interval. Thus, we should use

$$\Delta r < R\Delta\phi \tag{28}$$

Table 2. Speed-up factors achieved by the FFT method for computing A_i^H as compared to the termwise method

$\Delta\phi \times \Delta\lambda$	Factor
0.25° × 0.25°	23.48
0.30° × 0.30°	20.08
0.40° × 0.40°	13.49
0.50° × 0.50°	12.69

4.3 Interpolating high-degree accelerations

To achieve a consistent accuracy with that of the numerical integrator DVDQ (see Sect. 5.1), we used the Newton-Gregory forward polynomial (Gerald and Wheatley 1994) for interpolating A_i^H from the gridded values. Given $(n+1)$ equispaced data points $(x_i, f_i), i = 0, \ldots, n$, at an arbitrary x the interpolated value from the nth degree Newton-Gregory forward polynomial is (Gerald and Wheatley 1994)

$$P_n(x) = f_0 + \sum_{k=1}^{n} \binom{s}{k} \Delta^k f_0 \tag{29}$$

where $s = \frac{x - x_0}{h}$ with $h = x_{i+1} - x_i$, and

$$\binom{s}{k} = \frac{s(s-1)\cdots(s-k+1)}{k!} \tag{30}$$

$$\Delta^k f_0 = f_k + \sum_{j=1}^{k} (-1)^j \binom{k}{j} f_{k-j} \tag{31}$$

It can be shown that the error of $P_n(x)$ is (Shampine and Gordon 1975)

$$E(x) = \frac{(s)(s-1)(s-2)\cdots(s-n)}{(n+1)!} h^{n+1} f^{(n+1)}(\xi) \tag{32}$$

where ξ is in the smallest interval that contains $(x_0, x_1, \ldots, x_n)$. If x happens to be any of the knots x_i, then s will be an integer between 0 and n, thus making $E(x) = 0$ in Eq. (32). That is, the gridded values will be exactly reproduced. Given the position (r, ϕ, λ) of a satellite at any epoch, we first search for a cube that contains the grids of A_i^H and whose size is consistent with the specified polynomial degrees. Then, the three-dimensional interpolation is broken into three successive one-dimensional interpolations using the Newton-Gregory polynomial in the radial, and latitudinal and longitudinal directions (the result is independent of the order of interpolations). This successive method is frequently used in multidimensional interpolations, e.g. the polynomial interpolation in two dimensions described in Press et al. (1989). In theory, the three successive one-dimensional interpolations are not independent and a "rigorous" three-dimensional interpolation should use an interpolant with three variables.

To study the error of interpolation, we first form five grids of A_i^H using the following parameters:

$$\begin{aligned} &\text{Orbit: altitude} = 170\,\text{km, eccentricity} = 0.0007, \\ &\quad \text{inclination} = 60°, \text{Gravity field: model} = \text{EGM96}, \\ &\qquad N_{\max} = 360, S = 50 \end{aligned} \tag{33}$$

The orbital parameters in Eq. (33) have been used by Balmino and Barriot (1990). The radial range as computed from the degree-50 gravity field is about 30 km. The five grid types in Table 3 differ by their grid intervals. The choice of $\Delta r, \Delta\phi, \Delta\lambda$ follows the criteria in Eqs. (27) and (28). The product of the number of layers and Δr must be greater than the radial range. In fact, for the five grid types, grid intervals in r are much smaller than grid intervals in ϕ. For example, 5 km of Δr is much smaller than 0.25° of $\Delta\phi$ which is equivalent to 28 km along meridian. Since the radial range of a low orbiter is short, a small Δr will not yield a large number of layers that requires a large computer memory. Thus, we can use a small Δr and a low polynomial degree to carry out an accurate interpolation along the r direction and to reduce the computer time for interpolation. In this paper, the one-dimensional interpolations in the r direction will always use a polynomial degree which is equal to the number of layers minus 1, and the polynomial degrees mentioned below refer only to interpolations in the ϕ, λ directions. The required memory space for the five grid types should not pose any difficulty for an average computer. For example, the memory capacity of an average workstation can easily be expanded to 516 Megabytes using the virtual memory on a hard disk. Figure 2 shows that RMS relative errors of the interpolated A_i^H using the five grid types. The comparisons were made at a global 10° × 10° grid (total 648 data points) where the exact accelerations from termwise computations and the interpolated accelerations are available. In general, the higher the polynomial degree, the smaller the error. However, in most cases interpolations with polynomial degrees higher than 30 will result in numerical instability. The relative accuracies of the interpolations with grid types 3 and 4 can hardly be better than 10^{-4}, even with a polynomial degree of 29. Furthermore, the CPU time for interpolation increases quadratically with the polynomial degree.

Table 3. Grid type and required memory space of computer

Grid type	$\Delta\phi \times \Delta\lambda$	Δr (km)	No. of layers	Required memory (Megabyte)
1	0.25° × 0.25°	5	7	166.467
2	0.30° × 0.30°	5	7	115.647
3	0.40° × 0.40°	5	7	65.100
4	0.50° × 0.50°	5	7	41.685
5	0.30° × 0.30°	8	5	82.605

5 Case-study: fast trajectory integration for a low orbiter

5.1 The numerical integrator DVDQ and the true orbit

In this section, the proposed algorithm will be applied to integrating the trajectory of a low orbiter with the parameters specified in Eq. (33). We used DVDQ developed by Krogh (1969) as numerical integrator. DVDQ allows variable orders/step size in the integration according to error tolerances. Detailed formulae used in DVDQ can be found in Krogh (1974). Error analyses associated with DVDQ can be found in Shampine and Gordon (1975). The rectangular formulation is used to describe the equations of motion. Figure 3 shows the differences between the analytically computed orbit and the numerical integrated orbit in the two-body motion.

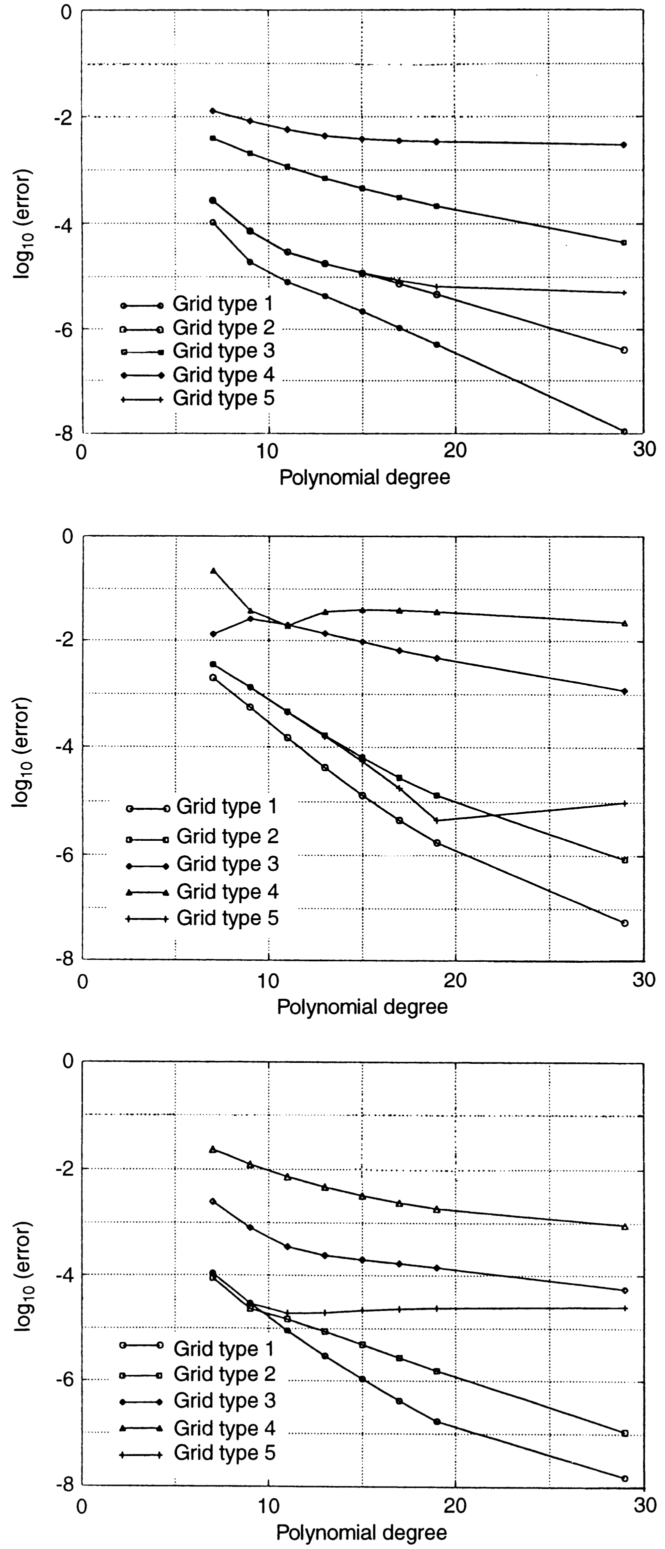

Fig. 2. RMS relative errors of the interpolated accelerations using the five grid types (see Table 3) for the radial component (top), the latitudinal component (middle) and the longitudinal component (bottom)

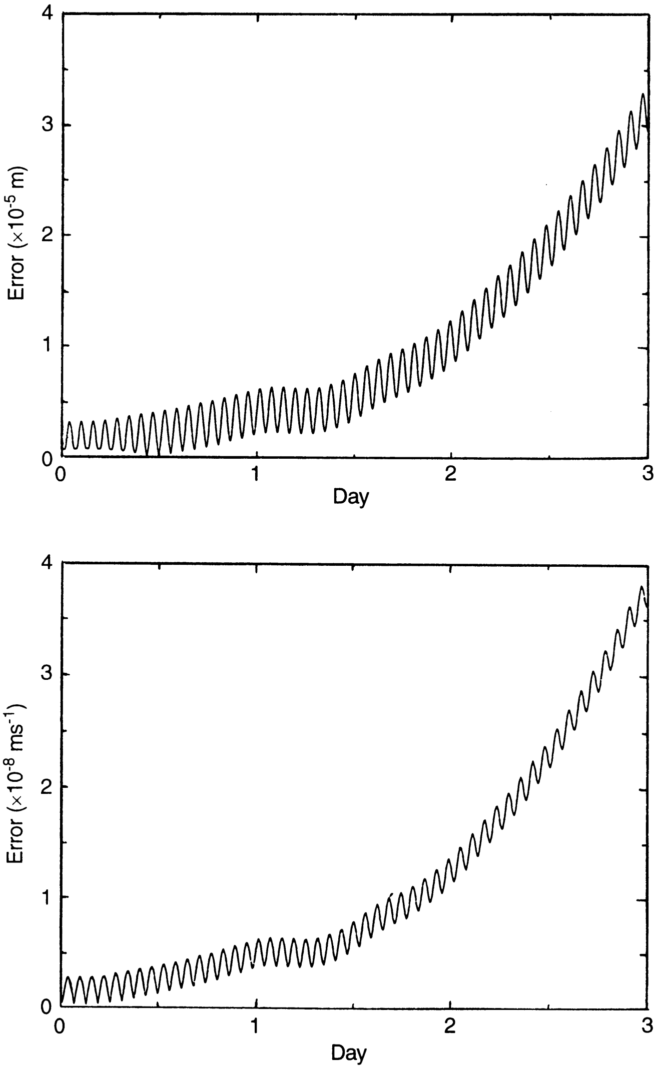

Fig. 3. The differences in position (top) and velocity (bottom) between the analytical orbit and the numerically integrated orbit for the low orbiter in the two-body motion

In this case the maximum errors in position and velocity are 3.3 × 10^{-5} m and 3.8 × 10^{-8} m/s, respectively, which, considering the magnitudes of position and velocity, have reached the limits of double-precision arithmetic (about 14 effective digits). This shows that DVDQ is a highly reliable integrator.

For comparisons, a 3-day "true" orbit was integrated using the conventional algorithm, which uses termwise computations to get the accelerations up to degree $N_{\max}$. The integration was carried out on a SUN SPARC5 machine and consumed 158.4 CPU h. Even on a fast, 64-bit-based DEC3000 machine, the integration took 55.2 CPU h. This proves that orbit integration with a high-degree gravity field is indeed a time-consuming computation. By comparison, the time needed for forming the grids for grid type 1 is 4415 CPU seconds (on SPARC 5), which is about 0.76% of the time for integrating the 3-day orbit.

5.2 Result of the proposed algorithm

Various "approximate" 3-day orbits were then computed with the high-degree accelerations interpolated from

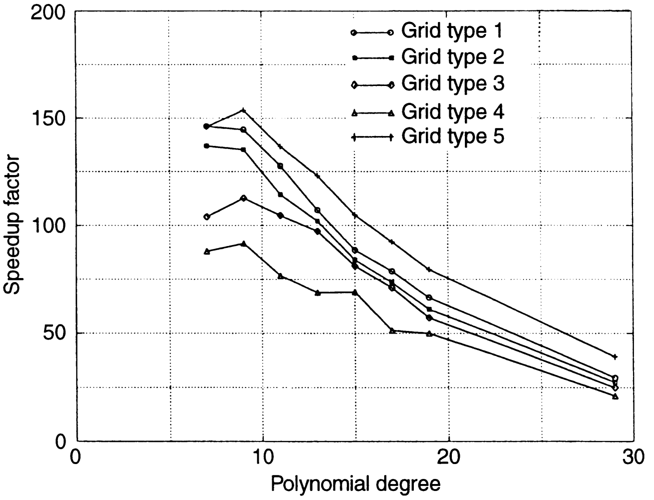

Fig. 4. Speed-up factors achieved by the new algorithm with different grid types and polynomial degrees

the five sets of gridded values in Table 3. For each grid type, various polynomial degrees were used. In the integrations we also employed the predict-pseudo correct algorithm (GTDS 1976). On average the predict-pseudo correct algorithm speeds up the orbit integrations by a factor of 1.82. Figure 4 shows the speed-up factors achieved by the new algorithm as compared to the conventional algorithm. The speed-up factors are governed by grid interval and polynomial degree. For a given polynomial degree, the speed-up factor decreases as the grid interval increases; for a given grid type, the speed-up factor decreases as the polynomial degree increases. The maximum errors of the "approximate" orbits, obtained by comparing with the 3-day "true" orbit, are given in Table 4. All maximum errors occur at the ends of the 3-day orbits. In general, the maximum errors decrease as the polynomial degree increases. For grid types 1, 2, 3, and 5, the maximum errors in position and velocity are of the order of 10^{-4} m and 10^{-7} m/s if the used polynomial degrees exceed 9, 11, 29, and 11, respectively. For grid type 4, a very high polynomial degree such as 29 will cause numerical instability and very large errors in position and velocity.

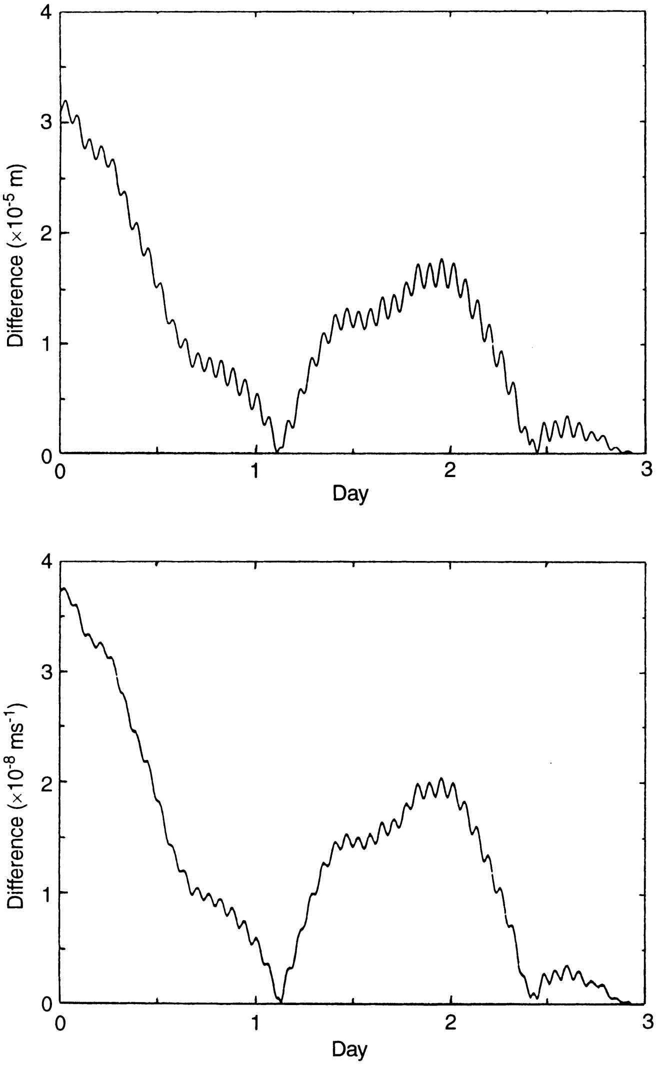

Fig. 5. The differences in position (top) and velocity (bottom) between the forward- and then backward-integrated orbits, the integrations use the new algorithm with grid type 1 and a polynomial degree of 9

When choosing a grid type, factors such as computer memory, speed-up factor, and the permissible error must be considered. For example, if one has no problem in computer memory and allows maximum errors of about 10^{-4}m and 10^{-7}m/s in position and velocity, one can use grid type 1 with a polynomial degree of 9 to achieve a speed-up factor of 145. Note that the maximum errors of 10^{-4}m and 10^{-7}m/s were adopted by Balmino and Barriot (1990) in their experiments on a

Table 4. Maximum errors in position and velocity of the approximate 3-day orbits (note: in each grid type, the first column is position error in m and the second column is velocity error in m/s)

Degree	Grid type 1	Grid type 2	Grid type 3	Grid type 4	Grid type 5
7	1.87e−3 2.14e−6	4.46e−3 4.96e−6	8.88e−2 1.03e−4	2.52e−1 2.98e−4	3.83e−3 4.20e−6
9	2.82e−4 3.19e−7	1.41e−3 1.57e−6	4.38e−2 5.10e−5	4.89e−1 5.76e−4	1.33e−3 1.47e−6
11	3.64e−4 4.29e−7	2.26e−4 2.59e−7	2.15e−2 2.50e−5	2.46e−1 2.88e−4	5.21e−4 5.87e−7
13	1.00e−4 1.17e−7	3.67e−4 4.25e−7	1.28e−2 1.50e−5	7.31e−2 8.18e−5	7.49e−4 8.79e−7
15	3.33e−4 3.94e−7	4.65e−4 5.51e−7	6.64e−3 6.91e−6	1.06e−1 1.22e−4	6.18e−4 7.33e−7
17	1.59e−4 1.86e−7	2.41e−4 2.87e−7	4.15e−3 4.90e−6	1.36e−1 1.58e−4	5.25e−4 6.25e−7
19	2.93e−4 3.45e−7	5.59e−4 6.64e−7	2.98e−3 3.54e−6	2.91e−1 3.36e−4	4.67e−4 5.56e−7
29	2.61e−4 3.09e−7	3.07e−4 3.63e−7	6.02e−4 7.16e−7	1.96e+1 2.32e−2	9.14e−4 1.08e−6

gradiometer mission. For this particular choice, the differences in position and velocity between the forward- and then backward-integrated 3-day orbits are computed and are plotted in Figure 5. With maximum differences of 3.1×10^{-5}m and 3.7×10^{-8} m/s in position and velocity, Figure 5 also demonstrates that both the numerical integrator DVDQ and the new algorithm are highly stable.

6 Conclusion

The proposed algorithm for orbit integration has been proved realistic for a case involving a low orbiter at an altitude of 170 km. On an average workstation, the computer time for integrating a 3-day orbit with a degree-360 gravity field can now be reduced to less than one CPU hour. When using single-precision arithmetic, the proposed algorithm may be used in Encke's method of orbit integration with a non-singular formulation of equations of motion to achieve the same level of accuracy as achieved by using the double-precision arithmetic. The proposed algorithm can also be used to compute the high-degree components of the six second-derivatives of the perturbing potential which are needed for integrating the variational equations (GTDS 1976, pp. 4–15). In such a case the required memory capacity will double that required for the acceleration components discussed in this work. Furthermore, for a highly eccentric orbit, the algorithm is still applicable, but will require more computer memory to store the grids that span a relatively large radial range. All programs described in this paper are freely available at the anonymous ftp site: gps.cv.nctu.edu.tw/pub/data/fast_orbit

Acknowledgements. This research is supported in part by the National Science Council of the Republic of China, under contract NSC86-2221-E009-065. We thank Dr. G. Métris for his excellent comments which improved the quality of this paper.

References

Balmino G, Barriot JP (1990) Numerical integration techniques revisited. Manuscr Geod 15: 1–10

Balmino G, Barriot JP, Valés N (1990) Non-singular formulation of the gravity vector and gravity gradient tensor in spherical harmonics. Manuscr Geod 15: 11–16

Colombo OL (1981) Numerical methods for the harmonic analysis on the sphere. Rep No 310, Dept Geod Sci Surv, Ohio State Univ, Columbus

CSR (1997) WWW site: http://www.csr.utexas.edu, Center for Space Research, Univ Texas at Austin

Gerald CF, Wheatley PO (1994) Applied numerical analysis (5th edn). Addison-Wesley, New York

GTDS (1976) Mathematical theory of the Goddard trajectory determination system. Greenbelt

Heiskanen WA, Moritz H (1967) Physical geodesy. Freeman WH, San Francisco

Hwang C (1998) Inverse Vening Meinesz formula and deflection-geoid formula: applications to the predictions of gravity and geoid over the South China Sea. J Geod 72: 304–312

Krogh FT (1969) VODQ/SVDQ/DVDQ – variable order integrators for the numerical solution of ordinary differential equations. TU Doc No CP-2308, NPO-11643, JPL, Pasadena

Krogh FT (1974) Changing the stepsize in the integration of differential equations using modified divided differences. In: Proc Conference on the numerical solution of ordinary differential equations. Dold A, Eckmann B (eds) Lecture notes in mathematics, vol 362. Springer, Berlin Heidelberg New York, pp 22–71

Lemoine FG, et al. (1997) The development of the NASA GSFC and NIMA joint geopotential model. In: Proc Int Symp Gravity, geoid, and marine geodesy. Segawa J, Fujimoto H (eds) Springer, Berlin Heidelberg New York, pp 461–469

Press WH, Flannery BP, Teukolsky SA, Vetterling WT (1989) Numerical recipes. Cambridge University Press, New York

Rapp RH, Wang YM, Pavlis NK (1991) The Ohio State 1991 geopotential model and sea surface topography harmonic coefficient model. Rep No 410, Dept Geod Sci Surv, Ohio State Univ, Columbus

Seeber G (1993) Satellite geodesy. Walter de Gruyter, Berlin

Shampine LF, Gordon MK (1975) Computer solution of ordinary differential equations. WH Freeman, San Francisco

Tapley BD (1989) Fundamentals of orbit determination. In: Sansó F, Rummel R (eds) Theory of satellite geodesy and gravity field determination. Lecture notes in earth sciences, vol. 25. Springer, Berlin Heidelberg New York, pp 235–260